REAL-TIME ULTRASONIC INVESTIGATION OF FIBER-MATRIX DEBONDING IN CERAMIC-MATRIX COMPOSITE

Shi-Chang Wooh and Isaac M. Daniel
Robert R. McCormick School of Engineering and Applied Science
Northwestern University, Evanston, Illinois 60208

INTRODUCTION

Limitations of ceramic materials such as brittleness, low tensile strength and low fracture toughness are being overcome with the introduction of ceramic matrix composites. The mechanical behavior of these fiber-reinforced composites strongly depends on the fiber-matrix bonding condition. If the bonding is too weak, there is poor stress transfer. On the other hand, for a case of very strong bond, the material behaves in a brittle fashion. Recently, photomicroscopic observations were made and the macroscopic behavior of the material was related to the failure mechanisms and damage development under loading [1]. However, this method is destructive, limited to damage on the surface only and cannot easily detect fiber-matrix debonding. Since fiber-matrix debonding is an important indicator of material response it is important to investigate it nondestructively. An effort was made to correlate macroscopic response with microscopic observations and real-time ultrasonic measurements in a unidirectional silicon carbide/glass ceramic composite under longitudinal tensile loading [2].

In this work, the same material was investigated by ultrasound in an attempt to correlate fiber-matrix debonding with the change in velocity of the polarized shear wave in the plane transverse to fibers.

FAILURE MODEL

Figure 1 illustrates a typical stress-strain curve and corresponding failure mechanisms. The curve shows four primary regions of interest (regions A through D). The initial region of the curve (A) is the linear elastic range where virtually no damage could be found. When the matrix cracks are initiated, the curve tends to bend to a plateau and the matrix cracks are multiplying in region B. In the middle of the plateau (C), matrix cracks are saturated and debond initiation occurs. The curve enters region D as the interfacial debonding is saturated. Fiber fractures are observed somewhere in this range of stress and the material finally fails globally. The stress-strain curve and the transverse shear modulus are predicted by the following analyses.

Review of Progress in Quantitative Nondestructive Evaluation, Vol. 12
Edited by D.O. Thompson and D.E. Chimenti, Plenum Press, New York, 1993

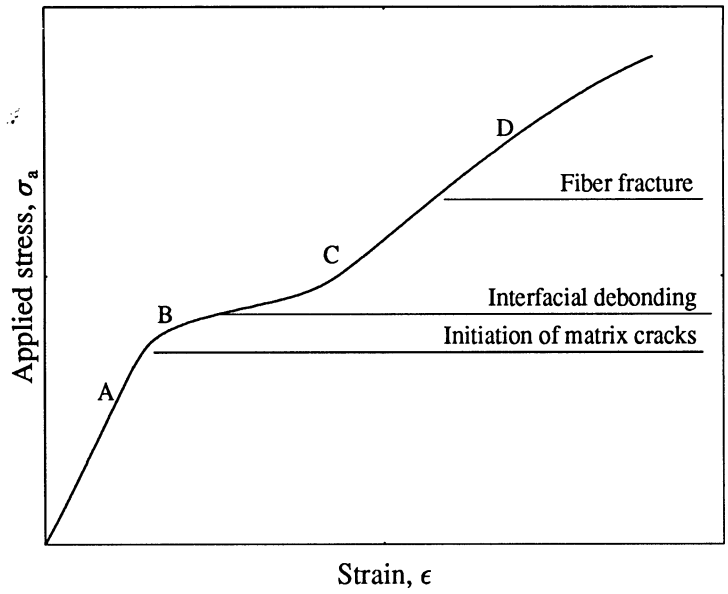

Fig. 1. Schematic illustration of stress-strain curve and failure mechanisms of unidirectional SiC/CAS composite.

Prediction of Stress-Strain Curve

A cylindrical brittle matrix element with a single fiber with two transverse matrix subjected to an axial tensile stress was considered [3]. Assuming that the fiber and matrix are perfectly bonded and the rate of change in the load carried by the matrix is proportional to the difference in average displacements of the matrix and fiber, the stresses between two cracks before and after debonding are calculated in terms of the constituent properties, applied stress, residual stress, crack spacing, and debond length. After calculating the residual stresses in the fiber direction from the stress-strain curve and applying the condition that matrix cracking occurs when the maximum tensile stress in the matrix reaches the tensile strength of the matrix, the crack spacing (ℓ) before debond initiation was computed as

$$\ell = \frac{2r_f \log\left(Q + \sqrt{Q^2 - 1}\right)}{\Gamma} \tag{1}$$

in which

$$Q = \frac{E_m\sigma_a + E_1\sigma_{rm}}{E_m\sigma_a + E_1(\sigma_{rm} - F_{mt})}$$

$$E_1 = E_f V_f + E_m V_m$$

and

$$\Gamma = \sqrt{\bar{H}\left(\frac{1}{E_f} + \frac{1}{E_m(\eta^2 - 1)}\right)}$$

$$\bar{H} = \frac{2}{\frac{1}{4G_f} + \frac{(3\eta + 1)(\eta - 1)}{3(\eta + 1)^2 G_m}}$$

$$\eta = \frac{1}{\sqrt{V_f}}$$

where E_f, E_m, G_f, G_m are respectively the moduli of fiber and matrix, V_f, V_m are the fiber and matrix volume fractions, σ_a is the applied stress, σ_{rm} is the residual stress in the matrix, and F_{mt} is the tensile strength of the matrix. In addition, the debond length (d) is obtained from the assumption that the interfacial shear stress at the tip of the debond is equal to the interfacial shear strength F_{is}:

$$\tau_i(d) = F_{is}$$

An explicit expression for the debond length can be obtained if interfacial friction is neglected:

$$d = \frac{1}{2}\left[\ell - \frac{r_f}{\Gamma}\log\frac{1+\xi}{1-\xi}\right] \tag{2}$$

where

$$\xi = \frac{2F_{is}}{\Gamma}\frac{1}{\eta^2 - 1}\frac{E_1}{E_m\sigma_a + E_1\sigma_{rm}}$$

The stress-strain behavior can be predicted by calculating average axial strains for the range of given applied stresses.

Shear Modulus Prediction

Ehselby's equivalent inclusion method is used to calculate the effective shear moduli [4]. For the case of perfect bonding, the transverse shear modulus G_{23}^0 is calculated from the relationship:

$$G_{23}^0 = \frac{G_{23}}{G_m} = \frac{G_m(1 - V_f) + G_{23f}(3 - 4\nu_m + V_f)}{G_m[1 + (3 - 4\nu_m)V_f] + G_{23f}(3 - 4\nu_m)(1 - V_f)} \tag{3}$$

where ν_m is the Poisson's ratio of the matrix. For the case of complete debonding, it is expressed as

$$G_{23}^1 = \frac{G_{23}}{G_m} = \frac{(1 - V_f)\phi}{(1 - V_f)\phi + 4(1 - \nu_m^2)\chi V_f} \tag{4}$$

where

$$\begin{aligned}\phi &= (1+\nu_m)[1+2(1-\nu_m)Q](1-V_f)^2 \\ &\quad + [4R+(3-2\nu_m^2-2\nu_m\nu_{12f})Q](1-V_f)V_f \\ &\quad + 4(1-\nu_m)(1-\nu_{12f}\nu_{21f})RQ(2+V_f)V_f\end{aligned}$$

$$R = \frac{(1+\nu_m)E_{1f}}{4(1-\nu_{12f}\nu_{21f})E_m}$$

$$Q = \frac{(1+\nu_m)E_{2f}}{(1-\nu_{12f}\nu_{21f})E_m}$$

$$\begin{aligned}\chi &= (1-V_f)^2 + \frac{1}{1+\nu_m}[Q(1-\nu_m\nu_{12f}) \\ &\quad + 4R(1-\nu_m\nu_{12f})]V_f(1-V_f) + \frac{1-\nu_m}{E_m}QE_{1f}V_f^2\end{aligned}$$

The transverse shear modulus (G_{23}) of a partially bonded material is then predicted by linear interpolation of the moduli for perfect bonding and complete debonding cases, i.e.,

$$\frac{G_{23}}{G_{23}^0} = 1 - \frac{2d}{\ell_d}\left(1 - \frac{G_{23}^1}{G_{23}^0}\right) \tag{5}$$

where ℓ_d is the crack spacing at debond initiation.

ULTRASONIC MEASUREMENTS

It was shown that the material properties of a unidirectional orthotropic laminate can be measured by means of ultrasonic wave propagation [5]. They are obtained from the Christoffel equation by solving the following determinantal equation:

$$\det\begin{vmatrix}\Gamma_{11}-\rho c^2 & \Gamma_{12} & \Gamma_{13} \\ \Gamma_{12} & \Gamma_{22}-\rho c^2 & \Gamma_{23} \\ \Gamma_{13} & \Gamma_{23} & \Gamma_{33}-\rho c^2\end{vmatrix} = 0$$

where Γ_{ij} are the Christoffel stiffnesses expressed in terms of material constants and directional cosines. By setting directional cosines for a wave motion traveling in the thickness direction, the transverse shear modulus is obtained as

$$G_{23} = \rho c_{23}^2 \tag{6}$$

where c_{23} is the velocity of the shear wave polarized in the plane transverse to the fiber direction. In practice, this wavespeed was measured in the quefrency domain by means of a technique called power cepstrum analysis [2]. This approach is computationally much easier and simpler than direct measurement in the time or frequency domain. In addition to the wavespeed measurements, attenuation due to damage was also measured from the signals of multiple reflections in the material [2].

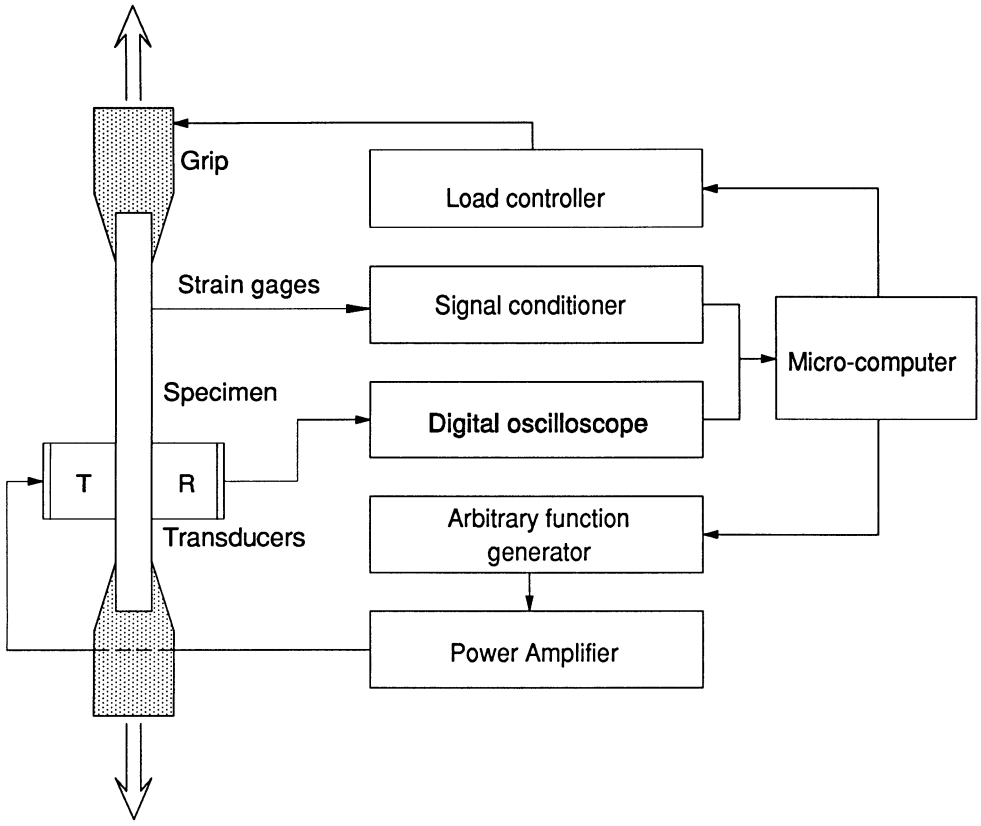

Fig. 2. Schematic block diagram of the ultrasonic system.

EXPERIMENTAL PROCEDURES

The material investigated was unidirectional SiC/CAS, calcium aluminosilicate glass ceramic reinforced with silicon carbide fibers, manufactured by Corning Glass Works. The fiber is silicon carbide yarn known as Nicalon (Nippon Carbon Co.) of 15 μm average diameter. The composite was obtained in the form of 16-ply, 3.048 mm (0.12 in.) thick unidirectional plates.

Figure 2 is a schematic illustration of the ultrasonic testing system. Mechanical characterization was performed by studying the stress-strain behavior under uniaxial tension. The specimen was loaded in a servohydraulic testing machine while applied stress and strains (both longitudinal and transverse strains) were monitored. Meanwhile, a pair of ultrasonic shear wave transducers were tightly attached to the surfaces of the sample for ultrasonic characterization. These transducers were setup in through-transmission mode and they were aligned to generate shear wave polarized perpendicualr to fiber direction. A micro-computer was used to control the entire process of load control and data acquisition. A toneburst signal generated by an arbitrary function generator (LeCroy 9100) excites the transmitter after passing through an RF power amplifier (ENI 325LA). Then, the transmitted multiple echoes were recorded by a digital oscilloscope (Tektronix RTD710) running at a sampling rate of 5 ns (200 MHz). Meanwhile the mechanical measurements were recorded through the signal conditioner. As soon as all the measurements were completed, the specimen was immediately loaded to the next step and this procedure was repeated until global failure of the specimen.

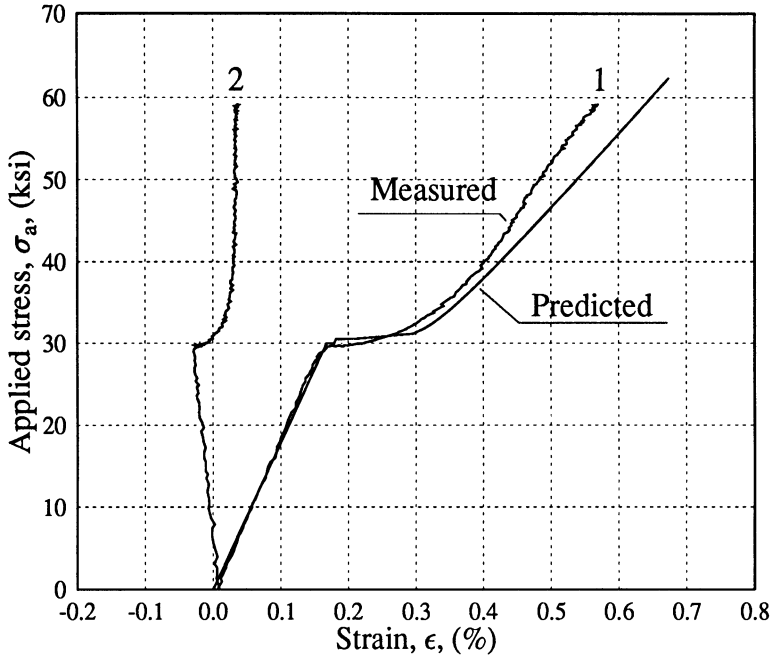

Fig. 3. Stress-strain curve for $[0_{16}]$ SiC/CAS specimen under uniaxial tensile loading.

RESULTS AND DISCUSSION

During uniaxial tensile loading, both longitudinal and transverse strains were recorded. Figure 3 is a typical stress-strain curve that shows the features corresponding to the failure mechanisms described previously. The predicted curve shows a good agreement with the measured curve up to the point of debond initiation. Fracture of fibers was not taken into consideration in the analysis and it is believed that the deviation between measurement and prediction in the last stage of the curve is due to this reason.

Figure 4 shows the change in normalized ultrasonic signal loss due to induced damage during loading as a function of applied strain. The signal loss (q) is directly related to the attenuation (α) by the relationship:

$$\alpha = -\frac{20}{h}\log(q) \tag{7}$$

where h is the specimen thickness. The attenuation shows a good qualitative correlation with the failure mechanisms as compared with the associated stress-strain curve (Fig. 3). The point of initial change in signal loss coincides exactly with the limit of the linear elastic region.

Figure 5 shows the predicted and measured variation of the transverse shear modulus G_{23} due to induced debonding during loading. It shows qualitatively that the modulus is

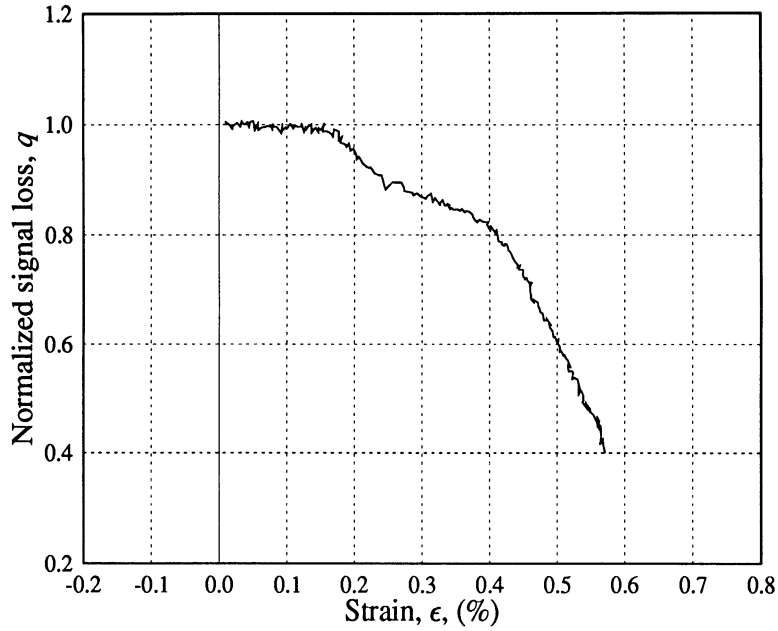

Fig. 4. Change in normalized signal loss due to induced damage during loading.

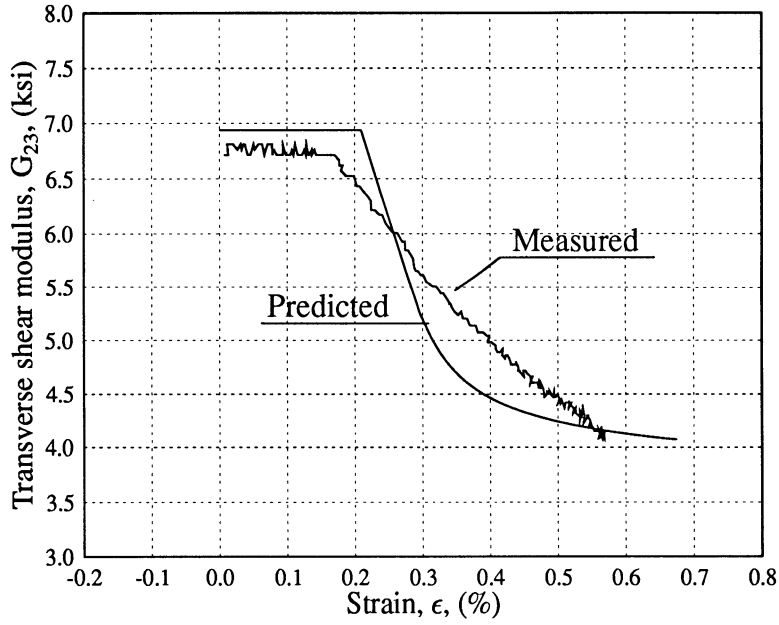

Fig. 5. Change in transverse shear modulus due to debonding during loading.

degraded as debonding grows. However, from the quantitative point of view, the experimental curve shows some deviation from the prediction. The rate of degradation of the experimental curve is more uniform compared to the prediction. This disagreement could be explained by the frictional force between the fiber and matrix. The friction prevents the sudden propagation of debonding immediately after initiation of debonds resulting in the less steep curve in this region. The agreement is better in the last part of the curve corresponding to more extensive debonding.

In summary, ultrasonic methods were developed for real-time monitoring of damage evolution in ceramic composites under tensile loading. The stress-strain curve was predicted analytically and shows a good agreement with the measurement. The transverse shear modulus calculated from wavespeed measurements was particularly sensitive to fiber-matrix debonding. Ultrasonic attenuation shows good qualitative agreement with the failure mechanisms and the combination of attenuation and wavespeed would be a useful method to study failure mechanisms. The effect of friction on debonding growth will be further investigated.

ACKNOWLEDGEMENT

This work was sponsored by the Air Force Office of Scientific Research (AFOSR). The authors are grateful to Dr. Walter F. Jones of the AFOSR for his encouragement and cooperation, to Mr. David Larsen of Corning Glass Works for supplying the material.

REFERENCES

1. Daniel, I. M., Anastassopoulos, G., and Lee, J.-W., "Experimental Micromechanics of Brittle-Matrix Composites," Micromechanics: Experimental Techniques, AMD-Vol. 102, ASME Winter Annual Meeting, San Francisco, CA, December 1989, pp.133–146.
2. Wooh, S. C. and Daniel, I. M., "Real-Time Ultrasonic Investigation of Damage Development in Ceramic-Matrix Composite," Review of Progress in Quantitative Nondestructive Evaluation, Vol. 11, eds. D. O. Thompson and D. E. Chimenti, Plenum Press, New York, 1992, pp.1523–1530.
3. Daniel, I. M., Anastassopoulos, G., and Lee, J.-W., "The Behavior of Ceramic-Matrix Fiber Composites under Longitudinal Loading," Composites Science and Technology, In press, 1992.
4. Takahashi, K. and Chou, Tsu-Wei, "Transverse Elastic Moduli of Unidirectional Fiber Composites with Interfacial Debonding," Metallurgical Transactions A, Vol. 19A, Jan. 1988, pp.129-135.
5. Wooh, S. C. and Daniel, I. M., "Mechanical Characterization of a Unidirectional Composite by Ultrasonic Methods," J. Acoust. Soc. Am., 90(6), 1991, 3248-3253.